# Study of damage evolution in composite materials based on the Thermoelastic Phase Analysis (TPA) method

DOI: https://doi.org/10.1016/j.compositesb.2017.02.040
COMPOSITES PART B: ENGINEERING post-print

# Study of damage evolution in composite materials based on the Thermoelastic Phase Analysis (TPA) method

Palumbo Davide, De Finis Rosa, Demelio Giuseppe Pompeo, Galietti Umberto

*Department of Mechanics, Mathematics and Management (DMMM), Politecnico di Bari, Viale Japigia 182, 70126, Bari, Italy*

*Corresponding author: Davide Palumbo, email: davide.palumbo@poliba.it, phone: 3495990841*

## Abstract

Standards and conventional procedures used for analysing fatigue damage in composite materials involve high experimental campaign costs due to time-consuming tests. This aspect becomes relevant for large structures where the cost of experimental setup tends to rise according to structure dimensions. In this regard, in recent years, efforts to produce fatigue characterisation of materials have made use of several experimental techniques, i.e. thermographic techniques. Most of these, however, refer to Standard specimens and laboratory equipment and set-up.

Through the use of Thermography, in this work a new procedure has been developed which is capable of monitoring damage in GFRP composite material. The analysis of thermal signal in the frequency domain allows for the isolation of indexes which are related to the thermoelastic and dissipative heat sources.

In particular, the phase of thermoelastic signal, associated with intrinsic dissipation processes occurring in the material, has been used to localize and assess the damaged areas in a quantitative manner. Moreover, the thermoelastic phase analysis leads to an evaluation of the endurance limit of composites. In fact, by comparing the results with those provided by the standard test methods, the

potential has been shown of the proposed procedure firstly as a non-destructive technique for continuous monitoring of damage in composite structures undergoing fatigue loadings, and secondly, as a fatigue limit index.

**Keywords:** GFRP, thermography, thermoelastic signal, TPA (Thermoelastic phase analysis), fatigue damage.

## 1. Introduction

Nowadays, composite materials play a key role in many engineering applications thanks to their light weight. In this regard, there are many examples of large structures or components made of composite material from boating-yachting to aeronautical or aerospace structures since a highly specific rigidity combined with a good mechanical behaviour are required [1], [2]. During their lifetime, after several loading cycles, these components need to be inspected in order to assess the presence of defects or damages that could compromise their residual mechanical strength. Standards propose procedures for the assessment of the fatigue performance of sample specimens which involves expensive and time consuming tests [3]. The cost of the experimental campaign increases when fatigue tests are carried out on a prototype or real component due to the high complexity of experimental apparatus.

Various experimental techniques and methods have been developed for the detection of damage in composites and metallic material during a fatigue test with the aim to reduce the testing time to a minimum [4-7]. Infrared Thermography is a non-destructive, full field and contactless technique capable of assessing fatigue damage by studying the heat sources generated during tests. In recent years, many authors have used InfraRed Thermography as an NDT technique in order to study the various damage phenomena rapidly and consistently [8-10]. In particular, several approaches and procedures based on the monitoring of temperature or heat source evaluation have been developed.

The temperature map of the specimen is used in the work of Saleem et al. [11] for investigating the effect of the machining process on the mechanical behaviour of composite plates with circular holes.

Montesano et al. [12] used a graphical method already verified by Luong [13] and Risitano [14] on metallic materials and based on the superficial temperature monitoring of the specimen during an incremental stepwise procedure. The stepwise procedure, as well illustrated in literature [14], involves considering several loading levels (starting at stress below the fatigue limit, up to failure of sample). Generally, each loading block, of a single test, runs with constant frequency and loading ratio. In this paper, the loading procedure is slightly different from the work [14] as will be showed furtherly.

In this case, the S-N curve obtained by using thermographic data, of polymer matrix composites (PMC) has been determined and an excellent correlation with the stress-life curve was obtained. Two different approaches (passive and active) have been applied in the work of Steinberger et al [15]. In particular, a quantitative characterization of damage has been performed by calculation of the loss factor via hysteretic heating.

Toubal et al. [16] showed the relation between the dissipation of heat and the damage of composites: three different stages have been observed during the damage evolution in composites CFRP open hole specimens. Similar results were obtained by Naderi et al. [6] during bending fatigue of Glass/Epoxy specimens. In an energetic approach [17], InfraRed Thermography was used associated with the acoustic emission technique to verify the dissipated energy evolution and damage process.

A different approach has been used by other authors [18], [19] e [20], [21] to investigate the damage phenomena in the material, based on a specific data processing of recorded infrared sequences. In this case, the temperature signal was analysed in the frequency domain so that the first and second order harmonics of the signal could be used to describe the nonlinear thermal signal component, due to the thermomechanical coupling phenomena. Kordatos et al. [22] used a

similar approach by combining InfraRed Thermography (dissipative heat source analysis) and acoustic emission techniques to study the fatigue behaviour of aluminium grade 1050 H16 and SiC/BMAS ceramic matrix composite cross-ply specimens.

In other works [23], [24], the potential of Thermoelastic Stress Analysis (TSA) for identifying small damages has been demonstrated. TSA is a non-contact, full field experimental technique which provides stress maps of a component subjected to dynamic loading [25-28]. This technique is based on the thermoelastic effect: a cyclically loaded component exhibits a small and reversible temperature change. In adiabatic and linear elastic conditions, these temperature changes are proportional to the first stress invariant. The procedures based on TSA have been developed in the last few years for the damage monitoring of standard specimens and complex shaped welded joints made of metallic materials (steel, titanium and aluminium) [29], [30].

TSA was used for evaluating the fatigue damage in composite materials in the works of Emery et al. [23], Fruehmann et al. [24] and Palumbo et al. [20]. In particular, in these works it has been demonstrated how damage mechanisms affect inner material producing a redistribution strains/stresses with consequent stiffness degradation. Moreover, during damage phenomena a departure from adiabatic conditions occurs in the through-the-thickness direction. These phenomena lead to a thermoelastic signal variation both in amplitude and phase. As shown in Palumbo et al. [20], in presence of damage, a significant thermal signal occurs at twice the loading signal related to the dissipative heat sources.

This work aims to show the capability of the Thermoelastic Phase Analysis (TPA) both to evaluate the fatigue limit and to study the damage behaviour of GFRP composites. To date, no information is present in literature referring to the use of TPA for the aforementioned purposes since the capability of TPA to detect damage, has been mostly discussed for metals.

The proposed approach is "passive", since no external heat sources are used for exciting the material. In this case, the material is subjected to an external loading in order to assess the

dissipative phenomena related to the damage. The main advantage with respect to the “active” approach is the opportunity to investigate the material (component) under actual loading conditions. The strong point of the proposed procedure lies with the possibility to obtain information about dissipative heat sources correlated to damage phenomena. The ability to localize the damaged areas has also been presented. In this regard, the main advantage is represented by the simple application and the much-reduced processing time of the proposed algorithm, which makes it very useful for the automatic scanning of large composite structures.

Furthermore, a parameter to determine the fatigue limit of the material has been presented: standard deviation of thermoelastic phase shift data. The use of standard deviation allows for a reduction in the processing time, since the subtraction of the phase map of initial loading level as a reference for undamaged conditions, is not required.

Moreover, since no difference between imposed sub-steps of specimens have been registered, several considerations lead to a validation of the test procedure for the tests on composites:

- The stepwise loading procedure is perfectly repeatable
- The stepwise loading procedure can be performed in less time, the time required to complete the first sub-step, without achieving 20,000 cycles.

## 2. Theory

Generally, during fatigue tests, two thermal effects are generated: thermoelastic heat sources and intrinsic dissipations. The first represents the well-known thermoelastic coupling while, intrinsic dissipation is thermodynamically irreversible. It is related to that part of mechanical energy dissipated as heat generated by the viscoelastic nature of the matrix material and other damage mechanisms that can be ascribed to frictional effects at fracture sites (matrix cracking, fibre fracture, and interface cracking /friction among other things [12]). The remaining part of mechanical energy is stored in material and represents the energy spent in fracture damage.

Under the hypotheses of adiabatic conditions, temperature changes $\Delta T_{el}$ for orthotropic materials are related to changes in the stresses in the principal material directions of the surface lamina [23, 31] by the following expression:

$$\Delta T_{el} = -\frac{T_0}{\rho C_p}\left(\alpha_1 \Delta\sigma_1 + \alpha_2 \Delta\sigma_2\right) \tag{1}$$

Where $\alpha_1$ and $\alpha_2$ are the coefficients of linear thermal expansion relative to the principal axes, $C_p$ is the specific heat at constant pressure, $\rho$ is the density, $T_0$ is the absolute temperature and $\Delta\sigma_1$and $\Delta\sigma_2$ are the stresses in principal directions.

The adopted acquisition systems of TSA, usually provide a non-radiometrically calibrated $S$ signal proportional to the peak-to-peak variation in temperature during the peak-to-peak variation of the sum of stress in principal directions. $S$ is usually presented as a vector, where modulus is proportional to the change in temperature due to the thermoelastic effect and the phase $\varphi$ means the angular shift between the thermoelastic and the reference signal [23]. In this work, we will focus our attention only on the uncalibrated signal since the proposed data analysis does not require the calibration procedure [31]. In this case, the following equation can be used:

$$A^* S = \left(\alpha_1 \Delta\sigma_1 + \alpha_2 \Delta\sigma_2\right) \tag{2}$$

where $A^*$ is a calibration constant.

The signal $S$ can be expressed in frequency domain as follows:

$$s_{th} = \frac{S}{2}\sin(\omega t + \pi + \varphi) \tag{3}$$

where $s$ is the non-calibrated thermoelastic signal, $\omega$ is the angular velocity and $\varphi$ is the phase angle between temperature and loading signal. In equation 3, the pi greek has been included in order to preserve the 'thermoelastic' phase shift between temperature and stress invariant.

This angle has a value different from zero in presence of the loss of adiabatic conditions and damage phenomena. In particular, in the event of damage occurring, non-linearity of thermoelastic signal and phase variations can be observed [24]. In linear elastic and adiabatic conditions, the phase shift between the temperature and the first stress invariant is 0° or 180°, depending on the sign of the first stress invariant and it can change with the presence of viscoelastic or damage phenomena that lead to the loss of adiabatic conditions. However, this parameter is also sensitive to external factors, which make the surface non-perfectly homogeneous such as non-homogeneity of the coating, surface defects or scratches or any other detectable surface modification.

As shown in Equation 3, the thermoelastic signal varies at the same frequency as the loading during the test.

It was demonstrated that the intrinsic dissipations occurred at twice the frequency of mechanical loading are two orders lower than the thermoelastic type [18], [22]. Moreover, the dissipative terms are irreversible sources unlike the thermoelastic type, causing an increase in the surface mean temperature of the specimen.

In effect, in the presence of damage, a typical three-stage trend is reported in surface temperature measurement [32]. Firstly, there is a mean temperature increase. Secondly, it reaches an equilibrium value due to balancing in dissipative sources and heat exchange effect [33]. Following the temperature plateau achieved, in the eventuality of failure occurring at a certain loading step, temperature will increase abruptly, as reported in [31].

In order to measure the surface temperature behaviour of the material undergoing fatigue loadings, and then to assess the phase shift of thermoelastic signal, a specific experimental setup and loading procedure have been adopted. In the following section, the experimental campaign as well as the

adopted processing technique will be presented, as a tool for evaluation of thermoelastic signal and its phase shift.

## 3. Experimental set-up

Twelve specimens were extracted from a laminate panel made of an epoxy-type resin reinforced with two external layers of cross-plied quasi-isotropic glass fibre +45°/0°/-45°/90° and two internal layers of unidirectional fibre of the 0° type. The fabrics are composed by multi-axial layers held together with a stitches thermoplastic yarn. Then, the material was moulded by a vacuum infusion technique.

The dimensions of the specimens were fixed according to Standard ASTM D 3039 which were 25 mm wide, 250 mm long and 2.5 mm thick [34]. All the specimens were tested on an MTS (model 370, 100 kN capacity) servo-hydraulic machine.

The S-N curves for estimating the fatigue limit have been applied to test seven specimen. In Table 1, the maximum stress applied adopting a stress ratio of 0.1 and a loading frequency of 7 Hz is shown.

The same fatigue test parameters were used for the thermographic tests. In this case, as shown in Table 2, a loading stepped procedure was performed starting with nominal stress amplitude ($\Delta\sigma/2$) of 30 MPa. At the end of each step (about 10,000 cycles of loading machine), the applied load was increased according to the values shown in Table 2.

The adopted experimental set-up for thermographic tests is shown in Figure 1.

An IR cooled In-Sb detector FLIR X6540 SC (640x512 pixel matrix array, thermal sensitivity NETD < 30 mK) has been used both to collect the thermal data and for the monitoring of superficial temperature of specimens. By adopting a 50 mm lens, a full-field view of the specimen has been obtained with a spatial resolution of 0.4 mm/pixel. The actual spatial resolution allows for detection of a wide part of a specific region of the surface material. Since the displacements of the composite

are very low (≤ 0.4 mm), they do not influence the post-processing analysis. Generally, significant displacements occur only at the final stress level (> 0.8 mm).

Referring to fixed stress level, three thermal sequences were acquired respectively at 2,000, 6,000 and 8,000 cycles, in order to investigate the damage within each loading step. These sequences in the paper will be indicated as Sub-step 1 (2,000 cycles), Sub-step 2 (6,000 cycles) and Sub-step 3 (8,000 cycles).

The adopted frame rate of the IR detector, was 100 Hz. Each acquisition lasts 10s; therefore 1,000 frames were recorded. Thermal sequences were analysed by Matlab® software.

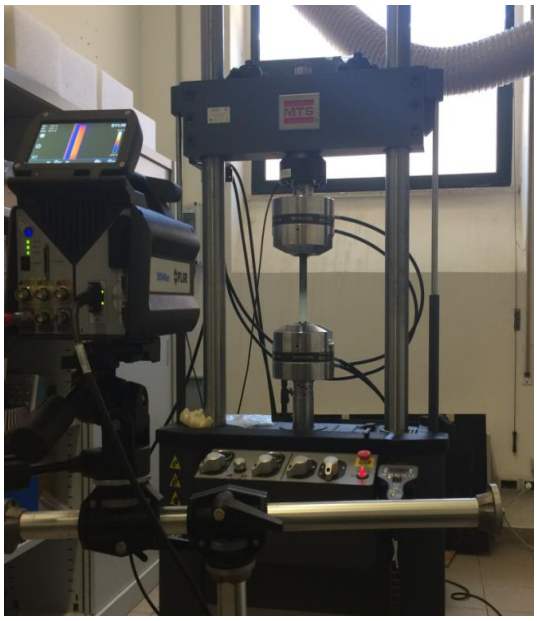

Figure1: Experimental set-up adopted for thermographic tests

| Step | σ max [MPa] | Number of cycles |
|---|---|---|
| 1 | 380 | 400 |
| 2 | 270 | 2,630 |
| 3 | 240 | 13,521 |
| 4 | 200 | 52,434 |
| 5 | 175 | 120,540 |
| 6 | 150 | 351,588 |
| 7 | 138.5 | 1,189,803 |

Table 1: Stresses and number of cycles to failure obtained on 7 specimens

| N | Δσ/2[MPa] | σ min [MPa] | σ max [MPa] | σ mean [MPa] |
|---|---|---|---|---|
| 1 | 30 | 6.7 | 66.7 | 36.7 |
| 2 | 35 | 7.8 | 77.8 | 42.8 |
| 3 | 40 | 8.9 | 88.9 | 48.9 |
| 4 | 45 | 10.0 | 100.0 | 55.0 |
| 5 | 50 | 11.1 | 111.1 | 61.1 |
| 6 | 55 | 12.2 | 122.2 | 67.2 |
| 7 | 60 | 13.3 | 133.3 | 73.3 |
| 8 | 65 | 14.4 | 144.4 | 79.4 |
| 9 | 70 | 15.6 | 155.6 | 85.6 |
| 10 | 75 | 16.7 | 166.7 | 91.7 |
| 11 | 80 | 17.8 | 177.8 | 97.8 |
| 12 | 95 | 21.1 | 211.1 | 116.1 |

Table 2: Number of loading steps and correspondent applied stresses

## 4. Methods and data analysis

A mathematical algorithm has been used to extract information pixel by pixel about parameters related to the surface temperature of the specimen, the signal amplitude and the phase of the thermoelastic signal. In particular, a suitable thermographic signal model has been used to study the thermal signal $S_m$ evolution (not radiometrically calibrated) in the frequency domain, as indicated in Equation (4):

$$S_m(t) = S_0 + at + S1\sin(\omega t + \varphi) \tag{4}$$

where the term $S_0 + at$ represents the increase in mean temperature during cyclic mechanical loading in terms of radiometric signal, $\omega$ is angular frequency of the mechanical imposed load, $S1$and $\varphi$ are respectively related to the amplitude and phase of thermoelastic signal.

Equation (4) was integrated in the algorithm of IRTA® software providing images in the form of data matrix for each constant parameter. In this work, the attention will be focused on the phase $\varphi$ and $S_0$ signals while the author draws the reader's attention to the work of Palumbo et al. [20] regarding the procedure and results obtained with *S1* signal.

The procedure for the processing of thermographic data was applied for each loading step and sub-step and provides:

- The acquisition of the thermographic sequence. About 1,000 frames were acquired for each sequence. In total, three sequences per loading level.
- Assessment of the three thermal signals: $S_0$ and $\varphi$ pixel by pixel (IRTA® software). It is worth noting that, in this case, no reference signal has been acquired simultaneously with thermal sequences and that IRTA software provided pixel by pixel the absolute value of the phase signal [30]. In other words, this means that the absolute value of phase varies for each loading step depending on the time chosen for the acquisition of thermal sequence (origin of the time sampling).
- Application of a Gaussian 2D-smoothing on IRTA® data matrix in order to obtain noise reduction. In this regard, the Gaussian kernel provides a gentler smoothing and preserves edges better than a similarly sized median kernel.
- Reduction of data matrix (area of analysis) to refer the analysis only to the gauge length area. In this case, the area of analysis was the same for $S_0$ and $\varphi$, (*A1* area, Figure 2) and includes 405x49 pixels.
- Subtraction of the environmental temperature influence on temperature signal $S_0$ achieved during each step and sub-step ($\Delta S_0$), which is required in order to obtain a good estimation of the damage-related temperature changes in material. Environmental temperature signal has been measured by using a dummy specimen (A2 area in Figure 2) [20]. The dummy specimen was set very closely to the sample undergoing the fatigue test.

- Evaluation of the 98th value of percentile to avoid outliers in temperature signal measurements ( $\Delta S_{0\_98perc}$ ) in the considered data matrix (A1 area). As stated by [20], since the energy of damage is proportional to the dissipated energy as heat per cycle, in order to closely follow the dissipation phenomena, the 98$^{th}$ percentile temperature value is chosen as a guideline [20]. Generally, the 98th percentile refers to a value series, in this case this calculation is applied to the pixel matrix of surface temperature. To assess the percentile values a suitable Matlab® function is integrated in the provided algorithm. The percentile rank formula is: $I_{98}$ = ((N+1)*K) / 100. $I_{98}$ represents the rank order of the score. K represents the percentile rank. N represents the number of scores in the distribution. The rank order of the score in this case provides the value to refer to for estimation of temperature value in the matrix at fixed loading level. Obviously, the value representative of the temperature will belong to $T_{min}$-$T_{max}$ data interval. This calculation makes sense in order to avoid outliers in determining the temperature value representative of the fixed loading level.

- Evaluation of the Standard Deviation (SD) of the thermoelastic phase signal $\varphi$ from the phase data matrix.

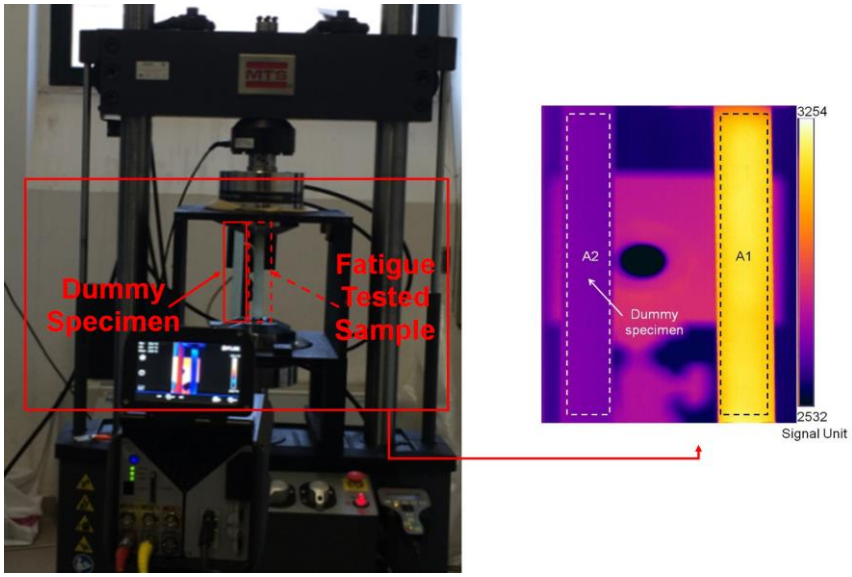

Figure 2: Area considered for analysis (A1) and for evaluation of environmental temperature signal (A2, dummy specimen)

The procedure used for the analysis of thermoelastic phase is shown in Figure 3 in a graphic flow-chart form.

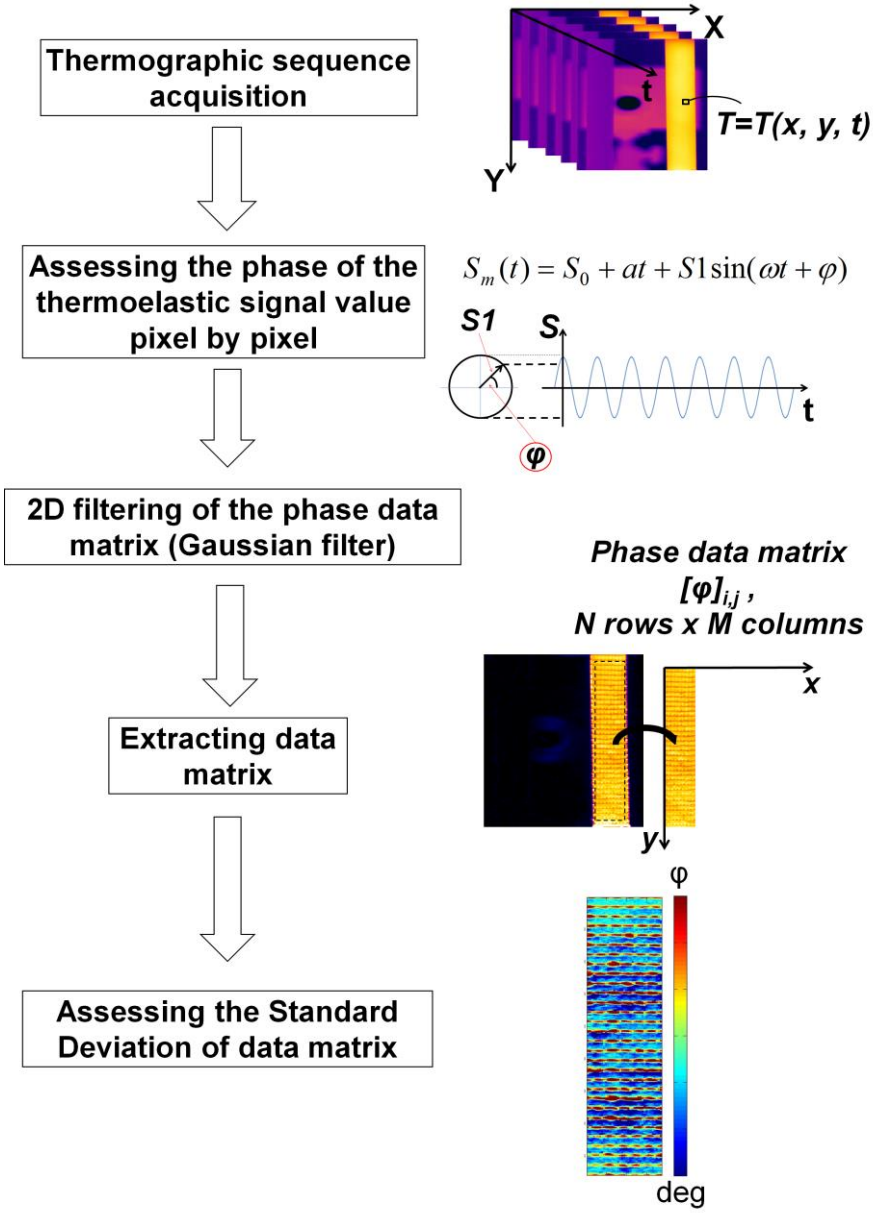


Figure 3: Flow chart of the proposed procedure

## 5. Results and discussions

In Figure 4, the convectional curve S-N obtained is shown with the data of Table 1 (7 specimens tested) which allows for the estimation of the fatigue limit of material for a higher number of cycles. To derive an interval estimation for subsequent observation, it would be appropriate to include in the graph in Figure 4, the 90% survival probability 'prediction straight lines' using a confidence interval of 95%, (dashed lines in Figure 4).

Considering a number of $2*10^6$ cycles as lifetime reference within High Cycle Fatigue a value of 124.89 MPa is extracted by data series, representing the fatigue limit in terms of $\sigma_{max}$ and of 56.20 MPa in terms of stress amplitude ($\Delta\sigma/2$).

Figures 5 a), 6 a) and 7 a) show the evolution of the temperature signal expressed as radiometric signal ($\Delta S_0$) for Specimens 2, 3 and 4 and for four different stress loading conditions (Sub-step 3). As stated in the previous section, this figure refers to the mean temperature trend during the stepwise procedure and has already been discussed by several authors [13], [14], [20].

In the same way, in Figures 5 b), 6 b) and 7 b) the maps of thermoelastic phase signal (Specimens 2, 3 and 4, Sub-step 3) are reported.

As already explained in the previous paragraph, the absolute value of phase signal varies between the loading steps and then, in order to compare the different phase maps, the mean value of the phase signal has been subtracted from each phase map (data matrix) according to the following equation:

$$[\varphi_m]_{N,M} = [\varphi]_{N,M} - \mathrm{mean}\{[\varphi]_{N,M}\} \tag{5}$$

where $[\varphi]_{N,M}$ is the phase data matrix of the *A1* area and $[\varphi_m]_{N,M}$ is the same matrix after subtracting its mean value. The phase mean value which was calculated and subtracted from matrix, refers to the data matrix $[\varphi]_{N,M}$ of a fixed loading level.

Both temperature (Figures 5a,6a,7a) and phase signal (Figures 5b,6b,7b) present a significant increase in damaged areas beyond the stress amplitude of 60 MPa. In particular, a correspondence is

very evident between the damaged areas (dashed lines) comparing temperature and phase signal, even if the latter provides more details and information about damage. As clearly evident in all phase maps, with respect to the first loading steps, phase signal experiences positive and negative value variations due to different mechanisms involved during fatigue loading. In particular, there is a well distinguished ordered pattern of horizontal stripes in the phase signal maps, which is very likely related to the morphology of the fabric of the surface lamina. In fact, phase signal increases in correspondence with the stitched thermoplastic yarn used in these fabrics to prevent crimping or undulations that can lead to loss of performance in the finished laminate. It is worth noting that the stitched yarns are visible also for lower values of imposed stress since they provide a different thermoelastic response with respect to the remaining part of the specimen. These stitches are fibres which are not aligned with the yarns and therefore, as also predicted by Eq. 1 and shown in [20], they give a different thermoelastic signal amplitude. In these areas, a different phase signal is probably due to a possible through-the-thickness heat leak between the stitches and the underlying fibre yarns due to very high temperature gradients. Consequently, the heat exchanges lead to the loss of adiabatic conditions and then to a positive phase shift over the stitches.

A phase signal delay characterizes (Figures 5b,6b,7b) the damaged areas of specimens as well illustrated in Demelio's work [21]. This delay, as well as thermoelastic amplitude , is correlated to the stiffness degradation with consequent strain redistribution in damaged areas. In fact, as described by other authors [35], the stiffness degradation is accompanied by an increase of the area of hysteresis loop and consequent phase lag between stress and strain. In particular, the strain is delayed with respect to stress and the phase lag increases as the fatigue damage increases.

In this regard, further works and other experimental techniques are necessary to relate the different damage mechanisms to the proposed thermographic procedure based on the monitoring of the phase signal.

Moreover, it is clear that the phase signal variation is effectively due to the yarn damage rather than to the effect of motion of the specimen. In fact, there are not evident differences between the upper part of specimen fixed to the static grip and the lower portion fixed to the dynamic one.

The trend of the signals evaluated with the proposed algorithm is shown in Figure 8 as a function of the amplitude stress for each sub-step. In particular, the radiometric temperature signal increases for each loading step due to the viscoelastic nature of the matrix material until a significant increase is verified in correspondence with the presence of the damage mechanisms, while the Standard Deviation of thermoelastic phase signal shows significant variations only for stress values above 55 MPa, Figure 9. In Figure 10, the same phase data are represented by omitting the last loading step. As already experimented for metallic materials [30], at first, the Standard Deviation of phase decreases as load increases and this is simply explained by a higher and better signal to noise ratio granted by higher load amplitudes. Subsequently, for a number of load steps, the phase is substantially stable. With the further increasing of loads, the SD tends to increase due to the damage phenomena.

Following the work of De Finis [32], in which a threshold method to evaluate the fatigue limit of metals was presented, Palumbo et al in their work [20], applied the method to total temperature $\Delta S_0$, thermoelastic and dissipative thermal components (respectively $\Delta S_1$ and $\Delta S_2$) of a GFRP composite specimen. For more details about this procedure, the reader can refer to the work of Palumbo.

By considering this typical trend of phase data, a new procedure has been developed to estimate the fatigue limit of material. For each specimen and for each sub-step, the adopted procedure consists of:

1. For $i=2:N-1$ with Step *1*, linear regression analysis of 3 data couples ($SD\_\varphi_{i-1}; \Delta\sigma/2_{i-1}$), ($SD\_\varphi_{i}; \Delta\sigma/2_{i}$), ($SD\_\varphi_{i+1}; \Delta\sigma/2_{i+1}$) and evaluation of the slope $m_i$ of the best fit line ($y=mx+q$). *N* represents the number of loading steps and $SD\_\varphi$ represents the Standard Deviation of the phase signal.
2. Point 1 provides the vector of the slope data of dimension (*N-2*).

3. Evaluation of the first loading step for which the condition: $(m\__i)_N>0$ is verified. The first loading step exceeding the condition is considered the estimation of fatigue limit. In this case, $m\__i$ are considered rounded to the nearest hundredth.

In this way, by considering Figure 10, the loading step that reaches the minimum value of Standard Deviation is considered to be the fatigue limit of material. Tables 3-7 show the results obtained for all specimens in each sub-step.

Figures 11 and 12 graphically illustrate the above procedures for Specimens 2, 3 and 4 at Sub-step 3. In particular, for the phase values, the slope values are plotted versus the stress amplitude and the dotted line represents the threshold value adopted for the estimation of the fatigue limit.

In Tables 8 and 9 the results (fatigue limits in terms of stress semi-amplitudes) for each parameter for temperature and phase signal at each sub-step are reported for five tested specimens.

By comparing the fatigue limits obtained by using $\Delta S_0$ and $\varphi$ data series, it is possible to observe that: temperature data allows for overestimation of the fatigue limit (60.67 MPa) with respect to the reference value 56.20 MPa, while the fatigue limit found by using $\varphi$ (52.00 MPa) seems to underestimate the value of SN reference. Nevertheless, the difference between the fatigue limit found by using both temperature and phase are similar enough to the reference. It is therefore possible to conclude that the results fit well with the S-N value reference as endorsed by the small standard deviation. Moreover, the phase of thermoelastic signal (52 MPa) provides more conservative values of fatigue limit with respect to temperature data.

As already shown in Figures 8 and 9, no difference exists between sub-steps. Hence, as shown in [20], an estimation of the fatigue limit could be very rapidly obtained with the proposed procedure since the thermographic data can be acquired at any time during the tests, while for the traditional procedure it is necessary to achieve steady state conditions before acquisition.

Finally, the small scattering between thermal parameters suggests that fatigue estimations obtained using thermal methods provide accurate results. The parameters provided by thermal methods converge to close estimations of a fatigue limit since they are associated to a considerably high

value of load cycles, specifically 2*10^6. This result makes such thermally derived fatigue limit estimations suitable for most engineering uses.

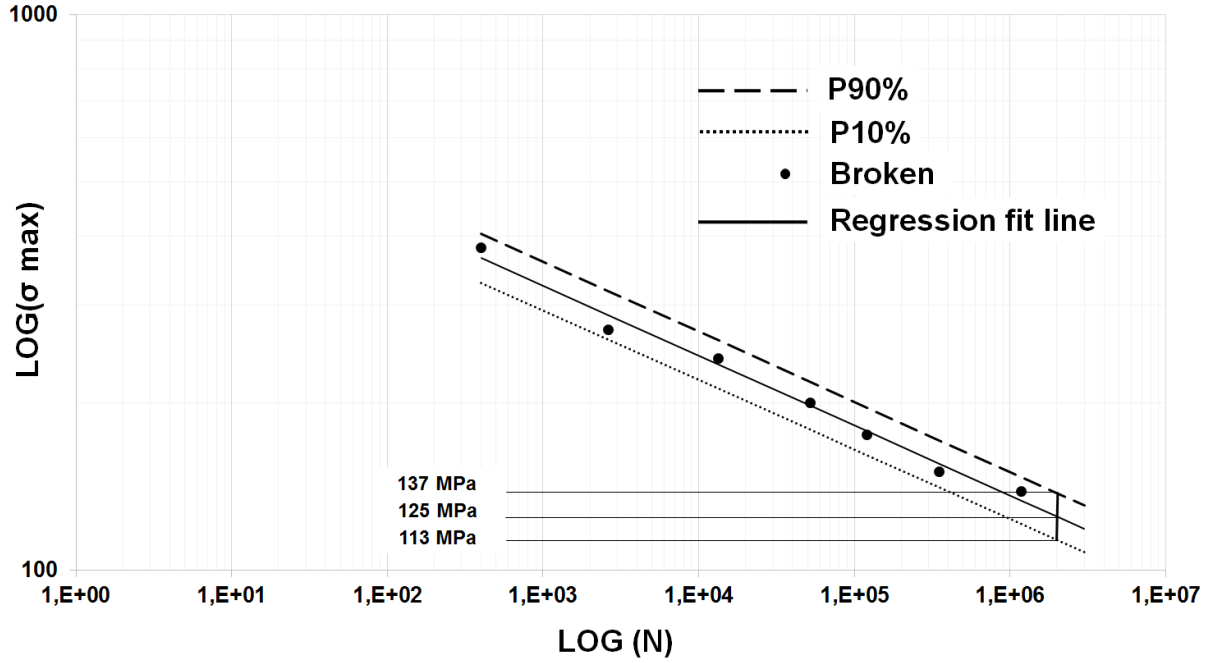


Figure 4: S-N curve and estimation of the fatigue limit in correspondence with a run-out limit of $2*10^6$ cycles.

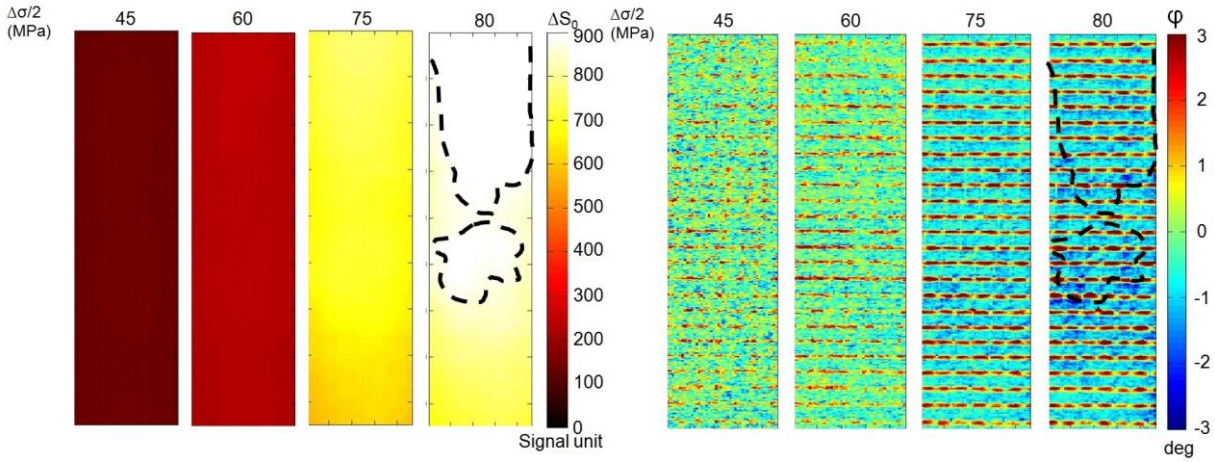


**(a)** **(b)**

Figure 5: Maps of radiometric temperature signal (a) and phase signal (b) obtained for 4 different loading steps, (Specimen 2, Sub-step 3)

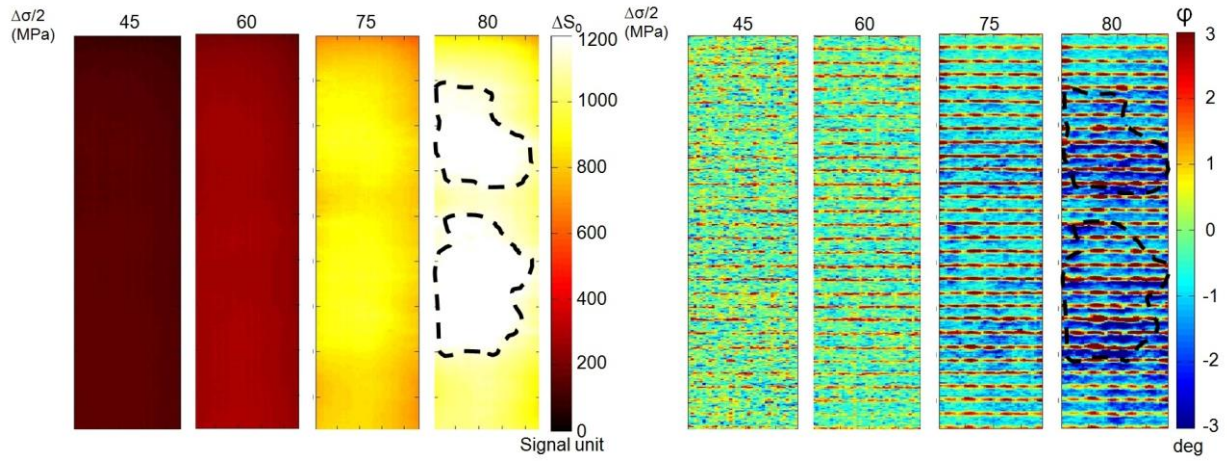


**(b)** **(b)**

Figure 6: Maps of radiometric temperature signal (a) and phase signal (b) obtained for 4 different loading steps, (Specimen 3, Sub-step 3)

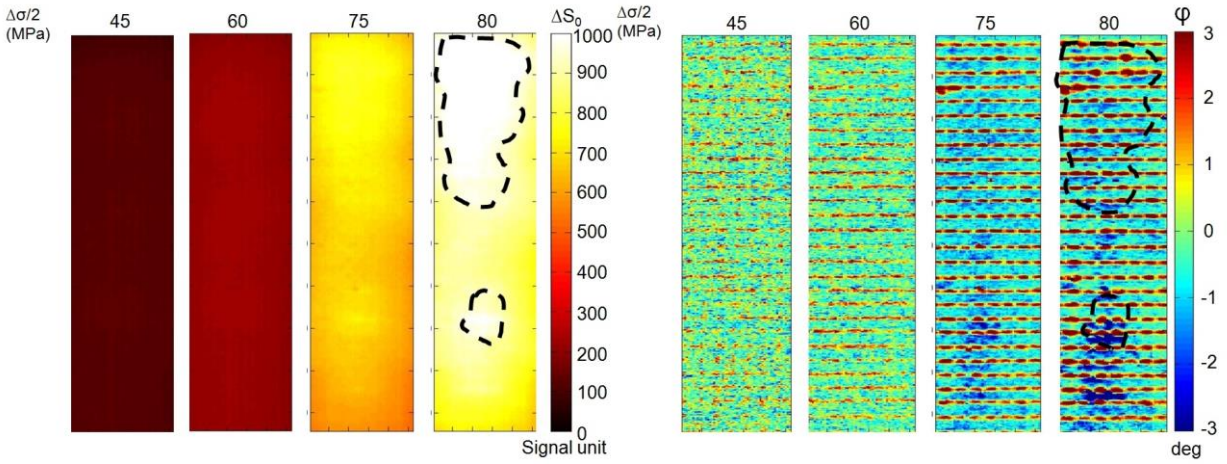


**(c)** **(b)**

Figure 7: Maps of radiometric temperature signal (a) and phase signal (b) obtained for 4 different loading steps, (Specimen 4, Sub-step 3)

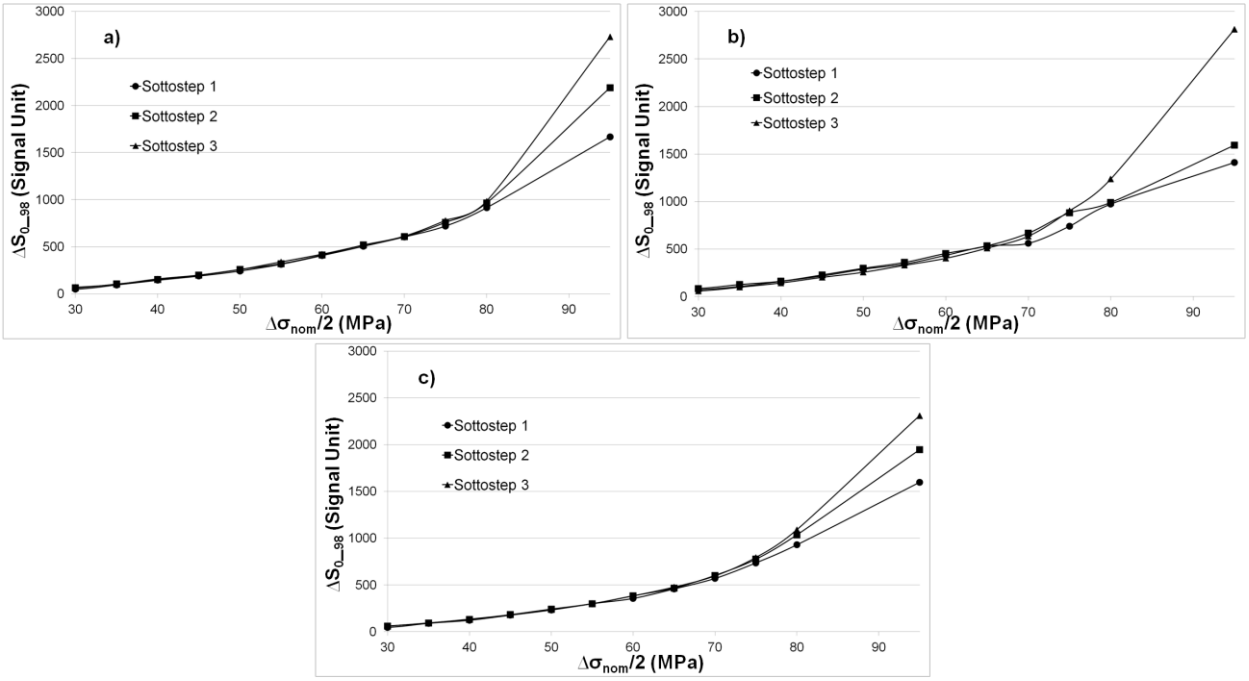


Figure 8: Thermographic signals expressed as radiometric uncalibrated signal obtained with proposed procedure as function of the amplitude stress for Specimens: a) 2, b) 3 and c) 4.

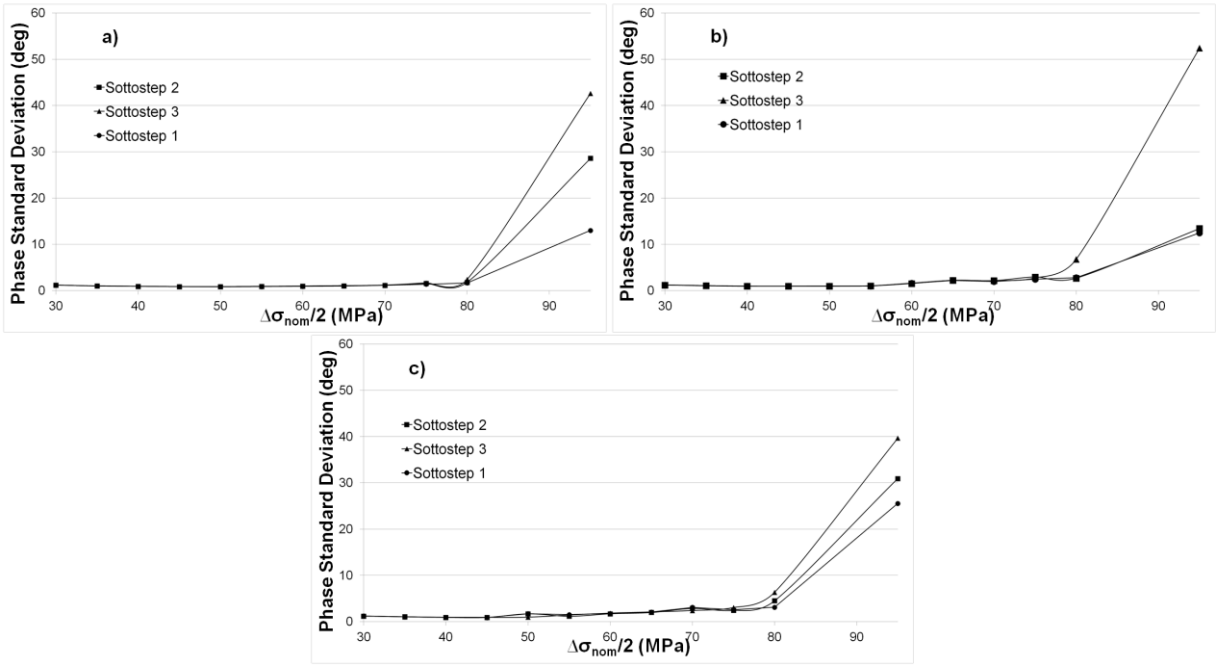


Figure 9: Standard Deviation of  phase signal obtained with proposed procedure as function of the amplitude stress for Specimens: a) 2, b) 3 and c) 4.

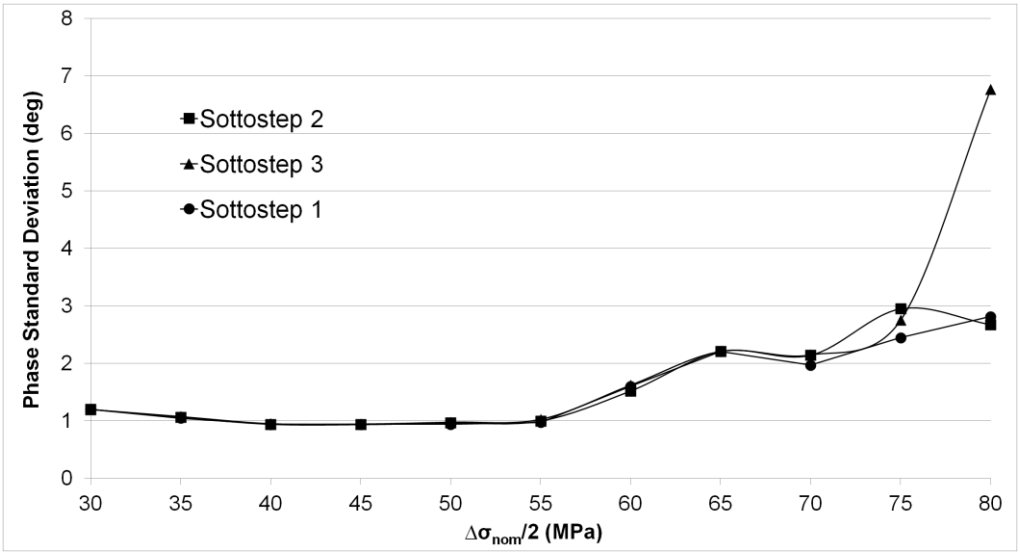


Figure 10: Standard Deviation of phase signal obtained with proposed procedure as function of the amplitude stress for Specimen 4.

| | | *sub-step 1* | | *sub-step 2* | | *sub-step 3* | |
|---|---|---|---|---|---|---|---|
| *N* | *Δσ/2 [MPa]* | *SD_φ_i [deg]* | *m_i* | *SD_φ_i [deg]* | *m_i* | *SD_φ_i [deg]* | *m_i* |
| *1* | *30* | *1.22* | - | *1.22* | - | *1.23* | - |
| *2* | *35* | *1.06* | *-0.03* | *0.92* | *-0.05* | *1.07* | *-0.03* |
| *3* | *40* | *0.95* | *-0.02* | *0.67* | *-0.02* | *0.93* | *-0.02* |
| *4* | *45* | *0.87* | *-0.01* | ***0.68*** | ***0.01*** | *0.88* | *-0.01* |
| *5* | *50* | *0.84* | *0.00* | *0.75* | *0.02* | ***0.87*** | ***0.01*** |
| *6* | *55* | ***0.86*** | ***0.01*** | *0.89* | *0.03* | *0.94* | *0.01* |
| *7* | *60* | *0.93* | *0.02* | *1.09* | *0.06* | *1.01* | *0.02* |
| *8* | *65* | *1.04* | *0.03* | *1.44* | *0.06* | *1.10* | *0.08* |
| *9* | *70* | *1.18* | *0.03* | *1.64* | *0.06* | *1.86* | *0.04* |
| *10* | *75* | *1.37* | *0.14* | *2.00* | *0.09* | *1.50* | *0.03* |
| *11* | *80* | *2.60* | *1.72* | *2.51* | *2.97* | *2.18* | *3.63* |
| *12* | *95* | *33.66* | - | *57.23* | - | *69.13* | - |

Table 3: Values of phase standard deviation (*SD_φ*) and slope (*m* ) of each loading level and sub-step, capable of estimating the fatigue limit of material (Specimen 1). In bold, the $m_i$ values for which the condition in Point 3 is verified.

| | | *sub-step 1* | | *sub-step 2* | | *sub-step 3* | |
|---|---|---|---|---|---|---|---|
| *N* | *Δσ/2 [MPa]* | *SD_φ_i [deg]* | *m_i* | *SD_φ_i [deg]* | *m_i* | *SD_φ_i [deg]* | *m_i* |
| *1* | *30* | *1.17* | - | *1.17* | - | *1.15* | - |
| *2* | *35* | *1.00* | *-0.03* | *1.00* | *-0.03* | *1.01* | *-0.03* |
| *3* | *40* | *0.91* | *-0.02* | *0.91* | *-0.01* | *0.90* | *-0.02* |

| | | | | | | | |
|---|---|---|---|---|---|---|---|
| *4* | *45* | *0.85* | *-0.01* | *0.86* | *-0.01* | *0.85* | *0.00* |
| *5* | *50* | *0.82* | *0.00* | *0.85* | *0.00* | *0.86* | *0.00* |
| *6* | *55* | ***0.86*** | ***0.01*** | ***0.89*** | ***0.01*** | ***0.90*** | ***0.01*** |
| *7* | *60* | *0.91* | *0.01* | *0.96* | *0.01* | *0.98* | *0.02* |
| *8* | *65* | *1.00* | *0.02* | *1.04* | *0.02* | *1.06* | *0.02* |
| *9* | *70* | *1.12* | *0.04* | *1.15* | *0.05* | *1.19* | *0.06* |
| *10* | *75* | *1.38* | *0.05* | *1.53* | *0.06* | *1.68* | *0.12* |
| *11* | *80* | *1.65* | *0.62* | *1.79* | *1.45* | *2.43* | *2.19* |
| *12* | *95* | *13.02* | *-* | *28.58* | *-* | *42.62* | *-* |

Table 4: Values of phase standard deviation (*SD_φ*) and slope (*m* ) of each loading level and sub-step, capable of estimating the fatigue limit of material (Specimen 2). In bold, the $m_i$ values for which the condition in Point 3 is verified.

| | | *sub-step 1* | | *sub-step 2* | | *sub-step 3* | |
|---|---|---|---|---|---|---|---|
| *N* | *Δσ/2 [MPa]* | $SD\_\varphi_i$ *[deg]* | $m_i$ | $SD\_\varphi_i$ *[deg]* | $m_i$ | $SD\_\varphi_i$ *[deg]* | $m_i$ |
| *1* | *30* | *1.21* | *-* | *1.20* | *-* | *1.19* | *-* |
| *2* | *35* | *1.01* | *-0.03* | *1.05* | *-0.03* | *1.03* | *-0.03* |
| *3* | *40* | *0.92* | *-0.01* | *0.91* | *-0.02* | *0.93* | *-0.01* |
| *4* | *45* | ***0.87*** | ***0.08*** | ***0.90*** | ***0.08*** | *0.91* | *0.00* |
| *5* | *50* | *1.70* | *0.06* | *1.69* | *0.03* | ***0.95*** | ***0.05*** |
| *6* | *55* | *1.52* | *0.00* | *1.16* | *0.00* | *1.41* | *0.09* |
| *7* | *60* | *1.73* | *0.05* | *1.69* | *0.08* | *1.84* | *0.07* |
| *8* | *65* | *2.06* | *0.14* | *1.97* | *0.12* | *2.09* | *0.06* |
| *9* | *70* | *3.08* | *0.05* | *2.85* | *0.05* | *2.40* | *0.09* |
| *10* | *75* | *2.56* | *0.00* | *2.42* | *0.16* | *3.04* | *0.39* |
| *11* | *80* | *3.11* | *1.23* | *4.49* | *1.50* | *6.33* | *1.92* |
| *12* | *95* | *25.55* | *-* | *30.91* | *-* | *39.65* | *-* |

Table 5: Values of phase standard deviation (*SD_φ*) and slope (*m* ) of each loading level and sub-step, capable of estimating the fatigue limit of material (Specimen 3). In bold, the $m_i$ values for which the condition in Point 3 is verified.

| | | *sub-step 1* | | *sub-step 2* | | *sub-step 3* | |
|---|---|---|---|---|---|---|---|
| *N* | *Δσ/2 [MPa]* | $SD\_\varphi_i$ *[deg]* | $m_i$ | $SD\_\varphi_i$ *[deg]* | $m_i$ | $SD\_\varphi_i$ *[deg]* | $m_i$ |
| *1* | *30* | *1.20* | *-* | *1.20* | *-* | *1.20* | *-* |
| *2* | *35* | *1.04* | *-0.03* | *1.06* | *-0.03* | *1.07* | *-0.03* |
| *3* | *40* | *0.94* | *-0.01* | *0.94* | *-0.01* | *0.95* | *-0.01* |
| *4* | *45* | *0.94* | *0.00* | *0.93* | *0.00* | *0.94* | *0.00* |
| *5* | *50* | *0.94* | *0.00* | ***0.96*** | ***0.01*** | ***0.97*** | ***0.01*** |
| *6* | *55* | ***0.97*** | ***0.07*** | *1.00* | *0.06* | *1.03* | *0.07* |
| *7* | *60* | *1.60* | *0.12* | *1.60* | *0.12* | *1.62* | *0.12* |

| | | | | | | | |
|---|---|---|---|---|---|---|---|
| *8* | *65* | *2.21* | *0.04* | *1.52* | *0.06* | *2.21* | *0.05* |
| *9* | *70* | *1.97* | *0.02* | *2.21* | *0.07* | *2.15* | *0.05* |
| *10* | *75* | *2.45* | *0.08* | *2.95* | *0.05* | *2.75* | *0.46* |
| *11* | *80* | *2.81* | *0.53* | *2.67* | *0.57* | *6.77* | *2.61* |
| *12* | *95* | *12.47* | - | *13.43* | - | *52.40* | - |

Table 6: Values of phase standard deviation ($SD\_\varphi$) and slope ($m$ ) of each loading level and sub-step, capable of estimating the fatigue limit of material (Specimen 4). In bold, the $m_i$ values for which the condition in Point 3 is verified.

| | | *sub-step 1* | | *sub-step 2* | | *sub-step 3* | |
|---|---|---|---|---|---|---|---|
| *N* | *Δσ/2 [MPa]* | $SD\_\varphi_i$ *[deg]* | $m_i$ | $SD\_\varphi_i$ *[deg]* | $m_i$ | $SD\_\varphi_i$ *[deg]* | $m_i$ |
| *1* | *30* | *1.20* | - | *1.20* | - | *1.19* | - |
| *2* | *35* | *0.98* | *-0.04* | *1.02* | *-0.03* | *0.94* | *-0.04* |
| *3* | *40* | *0.84* | *-0.02* | *0.85* | *-0.02* | *0.84* | *-0.01* |
| *4* | *45* | *0.76* | *-0.01* | *0.77* | *-0.02* | *0.81* | *-0.01* |
| *5* | *50* | *0.69* | *-0.01* | *0.69* | *0.00* | *0.71* | *-0.01* |
| *6* | *55* | *0.70* | *0.00* | ***0.73*** | ***0.01*** | ***0.74*** | ***0.01*** |
| *7* | *60* | ***0.74*** | ***0.01*** | *0.75* | *0.01* | *0.80* | *0.01* |
| *8* | *65* | *0.82* | *0.02* | *0.85* | *0.02* | *0.88* | *0.02* |
| *9* | *70* | *0.90* | *0.02* | *0.93* | *0.02* | *0.96* | *0.02* |
| *10* | *75* | *1.04* | *0.02* | *1.04* | *0.03* | *1.08* | *0.04* |
| *11* | *80* | *1.13* | *0.12* | *1.21* | *0.19* | *1.32* | *0.19* |
| *12* | *95* | *3.37* | - | *4.70* | - | *4.70* | - |

Table 7: Values of phase standard deviation ($SD\_\varphi$) and slope ($m$ ) of each loading level and sub-step, capable of estimating the fatigue limit of material (Specimen 5). In bold, the $m_i$ values for which the condition in Point 3 is verified.

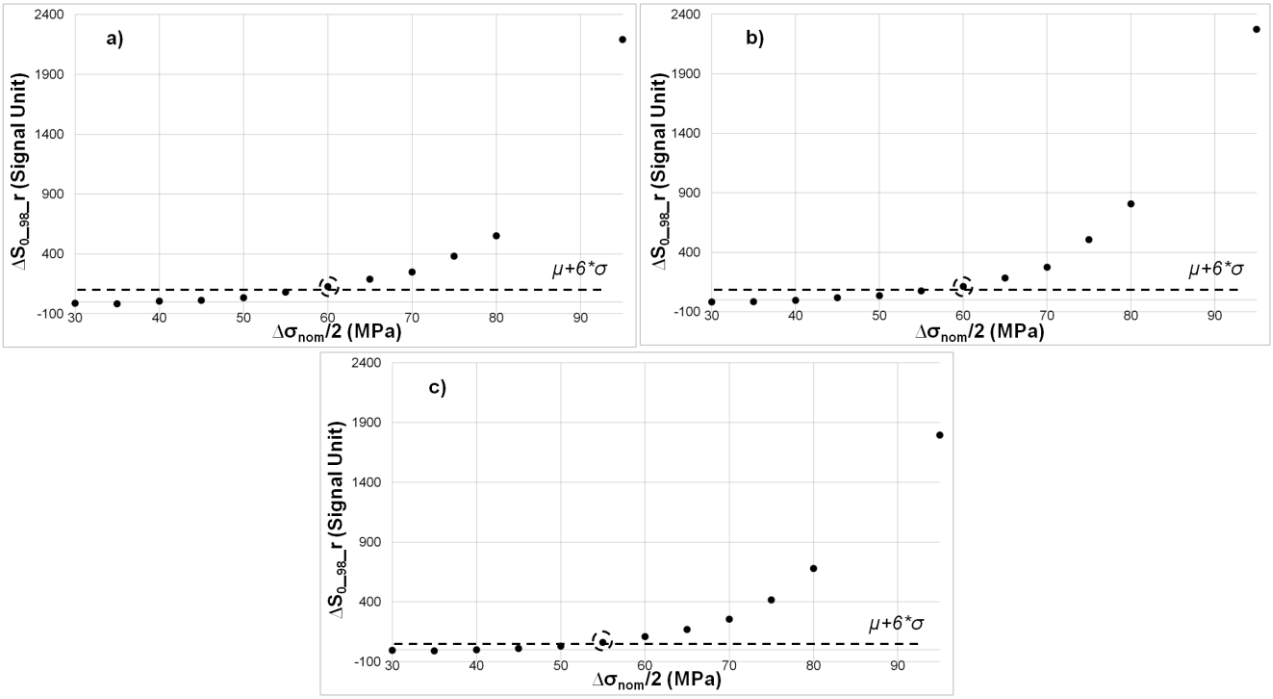


Figure 11: Estimation of the fatigue limit with the method [32] on temperature data, Sub-step 3, specimens: a) 2, b) 3 and c) 4.

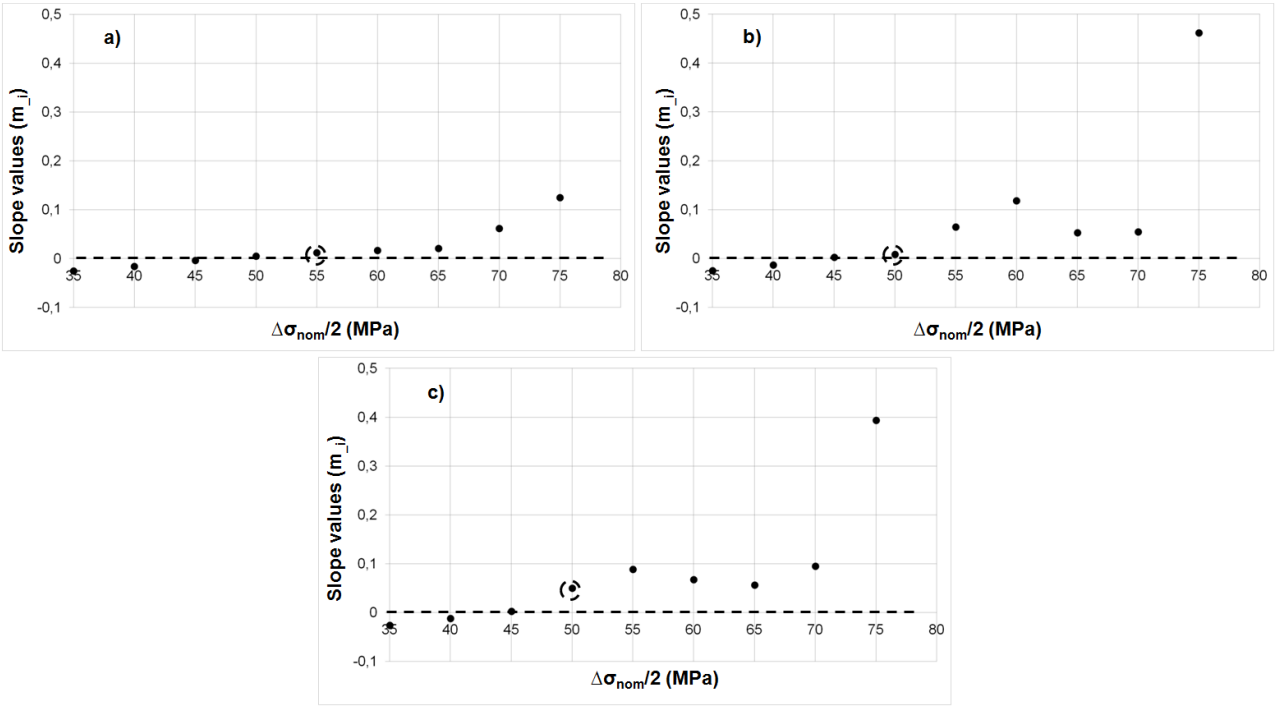


Figure 12: Estimation of the fatigue limit with the proposed method on SD of phase data, Sub-step 3, Specimens: a) 2, b) 3 and c) 4.

| N° Specimen | $\Delta S_{0\_98perc}$ (MPa) | | | |
|---|---|---|---|---|
| | *Loading sub-step 1* | *Loading sub-step 2* | *Loading sub-step 3* | **Average for specimen** |
| **1** | 60.00 | 60.00 | 60.00 | 60.00 |
| **2** | 60.00 | 60.00 | 60.00 | 60.00 |
| **3** | 60.00 | 60.00 | 60.00 | 60.00 |
| **4** | 70.00 | 65.00 | 65.00 | 66.67 |
| **5** | 60.00 | 55.00 | 55.00 | 56.67 |
| **Total Average** | **60.67** | | | |
| **Standard Deviation** | **3.72** | | | |

Table 8: Overall results accomplished by adopting the thermographic signal

| N° Specimen | *Phase Standard Deviation (MPa)* | | | |
|---|---|---|---|---|
| | *Loading sub-step 1* | *Loading sub-step 2* | *Loading sub-step 3* | **Average for specimen** |
| **1** | 50.00 | 50.00 | 50.00 | 50.00 |
| **2** | 55.00 | 55.00 | 55.00 | 55.00 |
| **3** | 45.00 | 45.00 | 50.00 | 46.67 |
| **4** | 55.00 | 50.00 | 50.00 | 51.67 |
| **5** | 60.00 | 55.00 | 55.00 | 56.67 |
| **Total Average** | **52.00** | | | |
| **Standard Deviation** | **4.14** | | | |

Table 9: Overall results accomplished by adopting the Standard Deviation of the phase signal

## 6. Conclusions

In this work, a novel procedure has been proposed for monitoring fatigue damage in GFRP composite materials with thermography. In particular, the phase of thermoelastic signal has been used to assess damaged areas during fatigue tests.

Twelve specimens were extracted from a laminate panel: seven of them were tested to assess S-N curves while five of them were tested in an ‘accelerated’ manner by performing the stepwise loading procedure in which each specimen underwent incremental loading levels until failure and three thermal sequences were acquired during each step in correspondence with three different

cycle numbers. Information about the thermal signal related to the increase of the mean temperature of the specimen and the phase of thermoelastic signal were obtained from processed data. Finally, a new method has been proposed for evaluating the fatigue limit of material at $2*10^6$ cycles.

By comparing the fatigue limits obtained by using S0 and φ data series it is possible to observe that : temperature data allows for overestimating the fatigue limit (60.67 MPa) with respect the reference value 56.20 MPa, while the fatigue limit found by using φ (52.00 MPa) seems underestimates the value of SN reference. Nevertheless, the difference between both the fatigue limit found by using temperature and phase are enough similar to the reference, then it's possible to conclude that the results fit well with the reference value.

The main considerations about the results obtained may be summarised as follows:

- the Standard Deviation of the phase signal can be used as a parameter to describe the fatigue damage in GFRP materials,
- no differences were observed between sub-steps (same loading step),
- results obtained with the proposed procedure show good agreement with those obtained by the S-N curve,
- an estimation of the fatigue limit may be obtained with the proposed procedure very rapidly since the phase data can be acquired at any time during the tests,
- as well as for metallic materials, phase signal provides local and more detailed information about the damaged areas.

Furthermore, the proposed procedure shows great potential as a non-destructive testing tool for the monitoring of real and more complex components undergoing actual loading conditions since no reference image is required for data analysis.

## References

[1]Bannister MK. Development and application of advanced textile composites. Proceedings of the Institution of Mechanical Engineers, Part L: Journal of Materials Design and Applications, 2004;218: 253-260.

[2]Palumbo D, Tamborrino R, Galietti U, Aversa P, Tatì A, Luprano VAM. Ultrasonic analysis and lock-in thermography for debonding evaluation of composite adhesive joints. NDT & E International, 2016;78:1-9.

[3]Harris B, Fatigue in composites. Cambridge: Woolhead Publishing Ltd, 2003.

[4]Munoz V, Valès B, Perrin M, Pastor ML, Welemane H, Cantarel A. Damage detection in CFRP by coupling acoustic emission and infrared thermography. Composites: Part B, 2016;85: 68-75.

[5]Goidescu C, Welemane H, Garnier C, Fazzini M, Brault R, Péronnet E, Mistou S. Damage investigation in CFRP composites using full-field measurement technique: Combination of digital image stereo-correlation, infrared thermography and X-ray tomography. Composites: Part B, 2013;48: 95-105.

[6]Naderi M, Kahirdeh A, Khonsari MM. Dissipated thermal energy and damage evolution of Glass/Epoxy using infrared thermography and acoustic emission. Composites: Part B, 2012;43:1613-1620.

[7]Kordatos EZ, Aggelis DG, Matikas TE. Monitoring mechanical damage in structural materials using complimentary NDE techniques based on thermography and acoustic emission. Composites: Part B, 2012;43: 2676-2686.

[8]Palumbo D, Ancona D, Galietti U. Quantitative damage evaluation of composite materials with microwave thermographic technique: feasibility and new data analysis. Meccanica, 2015;50, 443-459.

[9] Galietti U, Dimitri R, Palumbo D, Rubino P. Thermal analysis and mechanical characterization of GFRP joints. In: 15th European Conference on Composite Materials: Composites at Venice, ECCM 2012, Venice, Italy, 24-28 June, 2012.

[10] Tamborrino R, Palumbo D, Galietti U, Aversa P, Chiozzi S, Luprano VAM. Assessment of the effect of defects on mechanical properties of adhesive bonded joints by using non destructive methods. Composites Part B, 2016;91: 337-345.

[11] Saleem M, Toubal L, Zitoune R, Bougherara H, Investigating the effect of machining processes on the mechanical behavior of composite plates with circular holes. Composites: Part A, 2013, 55:167-177.

[12] Montesano J, Fawaz Z, Bougherara H. Use of infrared thermography to investigate the fatigue behavior of a carbon fiber reinforced polymer composite. Composite Structures, 2013;97:76-83.

[13] Luong MP. Infrared observation of thermomechanical couplings in solids. Thermosense XXIV Conference, part of SPIE's Aerosense 1-Orlando (Florida), 5 April, 2002.

[14] La Rosa G, Risitano A. Thermographic methodology for the rapid determination of the fatigue limit of materials and mechanical components. International Journal of Fatigue, 2000;22; 65-73.

[15] Steinberger R, Valadas Leitão TI, Ladstätter E, Pinter G, Billinger W, Lang RW. Infrared thermographic techniques for non-destructive damage characterization of carbon fibre reinforced polymers during tensile fatigue testing. International Journal of Fatigue, 2006;28: 1340-1347.

[16] Toubal L, Karama M, Lorrain B, Damage evolution and infrared thermography in woven composite laminates under fatigue loading. International Journal of Fatigue, 2006, 28:1867-1872.

[17] Meneghetti G, Analysis of the fatigue strength of a stainless steel based on the energy dissipation. International Journal of Fatigue, 2007, 29:81-94.

[18] Krapez JK, Pacou D, Gardette G. Lock-In Thermography and Fatigue Limit of Metals. Quantitative Infrared Thermography Journal, 2000;6:277-282.

[19] Ummenhofer T, Medgenberg J. On the Use of Infrared Thermography for the Analysis of Fatigue Damage Processes in Welded Joints. International Journal of Fatigue, 2009;31:130-137.

[20] Palumbo D, De Finis R, Demelio PG, Galietti U, A new rapid thermographic method to assess the fatigue limit in GFRP composites. Composites Part B, 2016, 103:60-67.

[21] Demelio PG, De Finis R, Galietti U, Palumbo D, Fatigue Limit Evaluation of Composite Materials by Means of TSA. QIRT Conference, July 4-8, 2016, Gdańsk, Poland.

[22] Kordatos EZ, Dassios KG, Aggelis DG, Matikas TE. Rapid evaluation of the fatigue limit in composites using infrared lock-in thermography and acoustic emission. Mechanics Research Communications, 2013; 54:14-20.

[23] Emery TR, Dulieu-Barton JK. Thermoelastic Stress Analysis of the damage mechanisms in composite materials. Composites: Part A, 2010;41:1729-1742.

[24] Fruehmann RK, Dulieu-Barton JM, Quinn S. Assessment of the fatigue damage evolution in woven composite materials using infra-red techniques. Composite Science and Technology, 2010;70:937-946.

[25] Harwood N, Cummings W. Thermoelastic stress analysis. New York: National Engineering Laboratory; Adam Hilger, 1991.

[26] Pitarresi G, Patterson EA. A review of the general theory of thermoelastic stress analysis. Journal of Strains Analysis, 2003; 38(5):405-417.

[27] Wang WJ, Dulieu-Barton JM, Li Q. Assessment of Non-Adiabatic Behaviour in Thermoelastic Stress Analysis of Small Scale Components. Experimental Mechanics, 2010;50:449-461.

[28] Palumbo D, Galietti U. Data Correction for Thermoelastic Stress Analysis on Titanium Components. Experimental Mechanics, 2016;56:451-462.

[29] Palumbo D, Galietti U. Characterization of Steel Welded Joints by Infrared Thermographic Methods. Quantitative Infrared Thermography Journal, 2014;11(1):29-42.

[30] Palumbo D, Galietti U, Thermoelastic Phase Analysis (TPA): a new method for fatigue behaviour analysis of steels. Fatigue and Fracture of Engineering Materials & Structures, 2016, in press, DOI: 10.1111/ffe.12511.

[31] Pitarresi G, Galietti U, A Quantitative Analysis of the Thermoelastic Effect in CFRP Composite Materials. Strain, 2010;46(5):446-459.

[32] De Finis R, Palumbo D, Ancona F, Galietti U. Fatigue Limit Evaluation of Various Martensitic Stainless Steels with New Robust Thermographic Data Analysis. International Journal of Fatigue, 2015;74: 88-96.

[33] Maquin F, Pierron F. Heat dissipation measurements in low stress cyclic loading of metallic materials: From internal friction to micro-plasticity. Mechanics of Materials, 2009; 41:928-942.

[34] ASTM D 3039/ D 3039M, Standard Test Method for Tension-Tension Fatigue of Polymer Matrix Composite Materials.

[35] Baxter T, Reifsnider K, The application of the Load-Stroke hysteresis technique for evaluating fatigue damage development. Proceedings of the American Society for Composites, September 20-22, 1994, Newark, Delaware.